ELSEVIER

Journal of Power Sources 58 (1996) 15–21

JOURNAL OF POWER SOURCES

Hydroxyl as a defect of the manganese dioxide lattice and its applications to the dry cell battery

H. Abbas [a], S.A. Nasser [b]

[a] *Physical Chemistry Department, National Research Centre, Dokki, Cairo, Egypt*

[b] *Physical Department, Faculty of Science Beni-Suef, Cairo University Beni-Suef, Cairo, Egypt*

Received 8 March 1995; revised 20 October 1995; accepted 20 October 1995

Abstract

Manganese dioxide polymorphs with different OH^- contents were prepared under various reaction conditions. X-ray diffraction measurements showed the presence of orthorhombic, tetragonal and hexagonal forms of MnO_2. Infrared absorption spectra in frequency range 200–4000 cm^{-1} of the different modifications were studied. The infrared absorption spectra showed the presence of hydroxyl groups in some forms of MnO_2 and the lack of such groups in other forms. The discharge behaviour and electrochemical activity of the prepared samples was determined in an electrolyte containing NH_4Cl and $ZnCl_2$. An attempt was made to correlate the structural parameters and OH^- content with the electrochemical activity of MnO_2 in the light of the cation vacancy model.

Keywords: Dry cell batteries; Manganese dioxide; Hydroxyl content

1. Introduction

The origin of the activity of manganese dioxide is a complex concept to define. This subject has attracted numerous research investigations in the field of dry cell technology. The activity of MnO_2 is influenced by its crystal structure, chemical composition, surface area, pore volume, pore-size distribution, morphological characteristics of the particles, density, presence of surface and bulk impurities, defect structure and content [1–7]. Burns and co-workers [8,9] suggested that naturally occurring and synthetic γ-MnO_2 phases used in batteries might contain lattice defects such as stacking faults, dislocations, chain defects, multi-dimensional tunnels and other irregular voids, and that water, as well as impurity ions, may be accommodated in such lattice defects. They stated that such defects might account for the high water content and high electrochemical activity of γ-MnO_2. Preisler [1] suggested that the water content influences the electronic band structure by deforming the rutile structure of β-MnO_2 and hence the Mn–Mn distances within the lattice. Desai et al. [5] stated that there is close correlation between the water content and electrode potential and that this relation would insist further investigation.

In view of this situation a number of synthetic MnO_2 samples with different crystalline modifications, and various OH^- ion contents have been prepared in order to estimate the influence of OH^- ions on the activity of MnO_2.

2. Experimental

2.1. Preparation of samples

MnO_2 with different degrees of oxidation and water contents were prepared under various reaction conditions [10]. The methods are summarized as follows.

2.1.1. Group A

A_1: Oxidation of a boiling solution of $MnSO_4$ (50 g/l) by $K_2S_2O_8$ solution (113 g/l). The latter was added dropwise under vigorous agitation. The resulting MnO_2 was decanted for 5 h, then filtered, washed and dried.

A_2: Oxidation of a boiling solution of $MnSO_4$ (50 g/l), acidified with 1 M H_2SO_4, using $(NH_4)_2S_2O_8$.

A_3: Electrodeposition from a solution containing 0.5 M $MnSO_4$ and 0.5 M H_2SO_4, at 20 mA/cm^2 and 90 °C, using platinum sheets as the anode and the cathode.

2.1.2. Group B

B_1: Preparation under the same condition as sample A_2 except that $K_2S_2O_8$ was used instead of $(NH_4)_2S_2O_8$.

B_2: Preparation by adding NH_4OH to $MnSO_4$ solution (57 g/l) until precipitation was complete. Oxidation of the product was carried out by $K_2S_2O_8$ (77 g/l) at pH 9.3.

B_3: Reduction of a boiling solution of $K_2S_2O_8$ (90 g/l) by HCl 1:1 (v/v).

SSDI 0378-7753(95)02770-9

C: Thermal decomposition of $Mn(NO_3)_2 \cdot 4H_2O$ in air at 250 °C.

2.2. Analytical methods

2.2.1. X-ray diffraction studies

X-ray diffraction (XRD) analysis was carried out with a Philips diffractometer (PW/1051), using Fe Kα radiation.

2.2.2. Infrared spectral studies

The infrared (IR) spectra in the range of 200–4000 cm^{-1} were taken on a Philips PU 9712 IR spectrophotometer using 5 mg powdered samples dispersed in KBr pellets.

2.2.3. Analysis

Chemical analysis of the investigated samples was carried out using standard methods reported in Ref. [11]. The total manganese and the amount of available oxygen were also determined [12]. The combined water content was determined by heating the sample (dried at 110 °C for 1 h) at 320 °C for 2 h and by determining the weight loss [13]. We have used the same temperature for all the samples. The choice of this particular temperature can be seen as arbitrary. In, fact we have adopted this procedure because the weight of a sample heated at 320 °C remains practically constant. Brenet et al. [13] found that the choice of the temperature 400 °C could give the weight loss that implied some loss of oxygen.

2.2.4 Density determination

Density was determined in a 25 ml pycnometer by displacement of toluene, using the density value 0.8604 g/cm^3 at 27 °C. Pycnometric-powder density measurements demand special precautions with respect to the gas included in the pores of the grains. According to Brown et al. [14], it is necessary to outgas the powder samples, in vacuum, prior to the addition of the pycnometer fluid, by means of degassed water. Small amounts of residual air in the pores can be dissolved in the outgassed water.

2.2.5. Discharge characteristics

The activity of the samples was determined using an electrochemical method described in Ref. [15]. The electrode was composed of 0.4 g Mn_2O and 0.1 g acetylene black. The discharge was carried out in an electrolyte solution containing 330 g $ZnCl_2$ and 200 g/l $NHCl_4$ (pH: 4.2) at a constant current of 30 mA/0.5 g. All measurements were carried out at room temperature.

3. Results and discussion

3.1. X-ray diffraction patterns

XRD patterns of MnO_2 samples are shown in Fig. 1. The *d*-values of the strongest reflections for samples A_1 to A_3

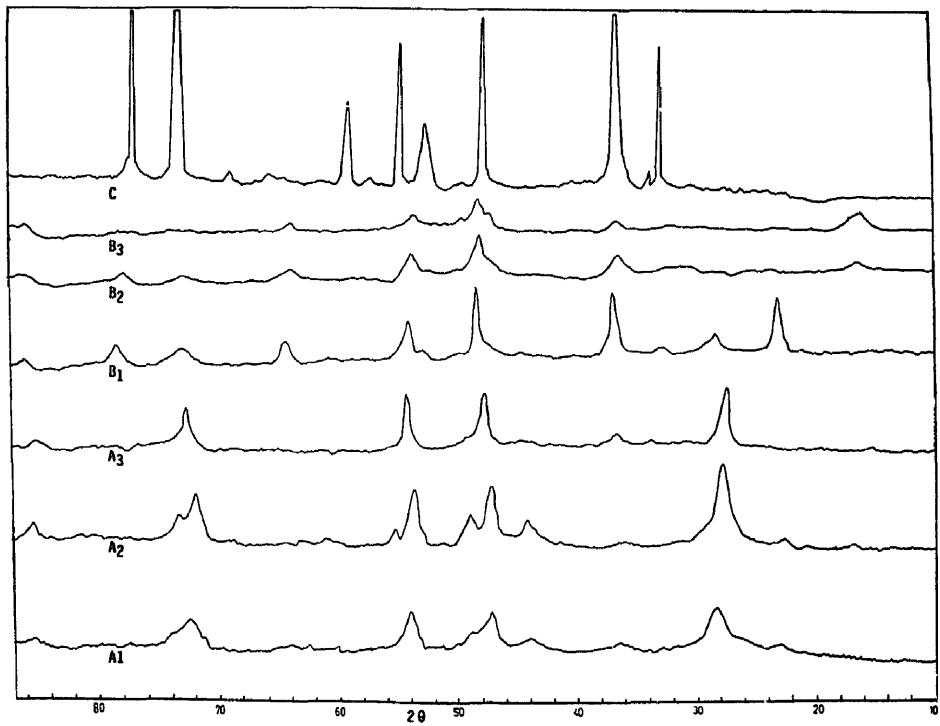

Fig. 1. X-ray diffraction patterns of manganese dioxide samples.

agree with ASTM data for γ-MnO_2 of the orthorhombic form [10]. It can be seen from Fig. 1 that there is a slight shift in the position of the diffraction lines, in addition to a change in intensity and broadening of the lines. The intensity of the diffraction peaks and their sharpness increases from sample A_1 to sample A_3.

It is well established that changes in peak position and relative intensity and/or broadening of XRD lines may be due to lattice imperfections. According to a results, it can be concluded that the number of lattice defects decreases gradually for orthorhombic γ-MnO_2 from samples A_1 to A_3.

Samples B_1, B_2, B_3 and C are identified as tetragonal (B_1), hexagonal (B_2 and B_3) and tetragonal (C) phases of MnO_2, corresponding to α-, δ- and γ-MnO_2, respectively. The sharpness of the XRD lines of β-MnO_2 (C) indicates that its crystallinity is high, and contains, therefore, fewer lattice defects. The poor crystallinity of δ-MnO_2 may be due to lattice imperfections, related to a high water content.

3.2. *Infrared absorption spectra*

IR absorption spectra of the various MnO_2 are shown in Fig. 2. The IR spectra of γ-MnO_2 samples A_1, A_2 and A_3 have one feature in common, namely characteristic broad absorption bands in the wave number range 324–580 cm^{-1}. The α- and β-MnO_2 samples are characterized by absorption bands around 480, 530, 700 and 330, 409 cm^{-1}, respectively.

The appearance of weak absorption bands at ≈470 and ≈700 cm^{-1} for the γ-MnO_2 samples was attributed to the presence of small traces of α-MnO_2. These data are in agreement with those reported in previous studies on IR absorption spectra [16,17].

The IR absorption spectra of the investigated samples show a strong absorption band at ≈1100 cm^{-1}, which may attributed to hydrogen bonding [16] and/or the MnO_2 stretching mode [18]. IR spectra are helpful in locating the presence of –OH grapes as well as water molecules that may be present as bound water within the crystal structure. γ-MnO_2 samples are characterized by absorption bands around 3400 and 1620 cm^{-1}, corresponding to the stretching and bending vibrational modes, respectively, of OH groups [16,17]. α-MnO_2, exhibiting absorption around 3400 cm^{-1}, does not show an absorption band around 1620 cm^{-1}. This suggests that the OH groups are linked in a different manner in the α-MnO_2 crystal structure [16,17]. In the case of δ-MnO_2 samples, bands are visible at 3400 and 1620 cm^{-1}, as well as an additional band at 1380 cm^{-1}, which is characteristic for this variety [19].

The absorption bands corresponding to OH group are absent for β-MnO_2.

3.3. *Chemical composition and water content*

The presently accepted formula for MnO_2 which contains structural water is proposed by Ruetschi [20] in the form $MnO_2 \cdot (2-n+m)H_2O$. The chemical composition and the

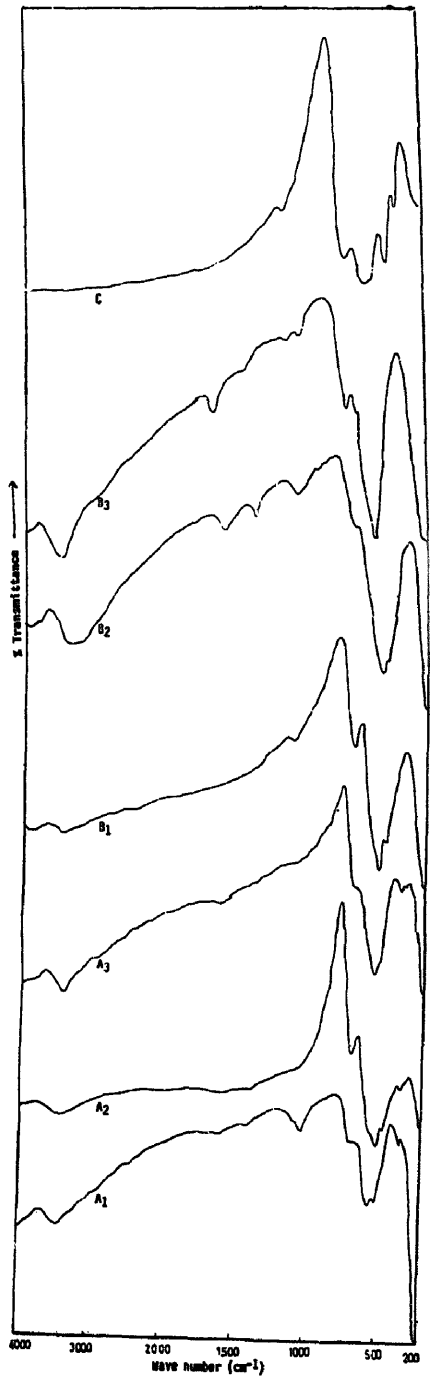

Fig. 2. Infrared spectra of manganese dioxide samples.

corresponding formula of the various MnO_2 samples are calculated on the basis of the cation vacancy model [20]. This model leads to the following formula:

$$Mn_{1-x-y}^{4+}Mn_y^{3+}O_{2-4x-y}^{2-}OH_{4x+y}^{-} \quad (1)$$

The parameters x (fraction of Mn^{4+} ions missing in the Mn^{4+} sublattice) and y (fraction of Mn^{4+} ions replaced by Mn^{4+}) in Eq. (1) are related to parameters n (degree of oxidation) and m (number of neutral molecules) by the set of equations:

$$x = m/(2+m) \quad (2a)$$

$$y = 4(2-n)/(2+m) \quad (2b)$$

The calculated values of n, m, x and y are given in Table 1. The variation in the oxidation degree n is due to partial replacement of O^{2-} and Mn^{4+} by OH^- and Mn^{3+}, respectively. The quantity of Mn^{3+} ions determines the value of n. The difference between m value for the various samples is more pronounced. The highest and lowest values of m and x are exhibited by the δ- and β-MnO_2 samples, respectively. Regarding the γ-MnO_2 samples, the values of m and x decrease gradually from samples A_1 to A_3. This may be due to the different preparation methods, e.g. the reaction conditions. The linear relation between the structural water content and the cation vacancy fraction is shown in Fig. 3(a). The quantity of Mn^{3+} (y) of the various MnO_2 samples is represented in Table 1. The data show that the concentration of trivalent Mn^{3+} ions tends to increase in the order β-<γ-<α-<δ-MnO_2.

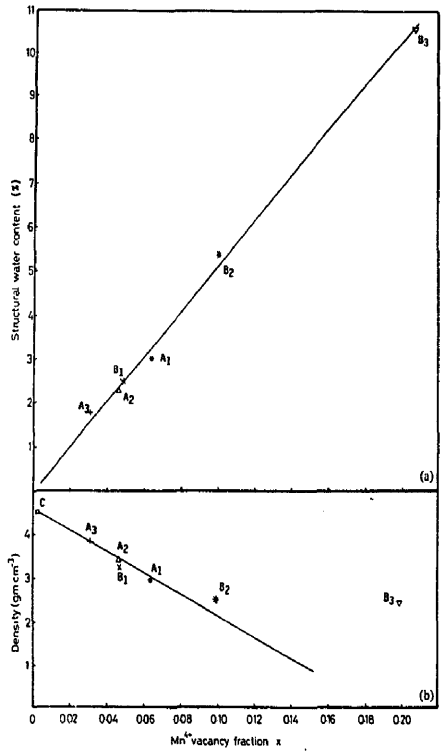

Fig. 3. (a) Structural water content (%) as a function of Mn^{4+} vacancy fraction x. (b) Density as a function of Mn^{4+} vacancy fraction x for the MnO_2 samples. (⊙) A_1, (△) A_2, (+) A_3, (×) B_1, (*) B_2, (▽) B_3, and (□) C.

3.4. Density

Density is one of the characteristic properties of materials that can be used for the identification of lattice defects [21]. Fig. 3(b) illustrates the pycnometric density of the various MnO_2's. The values obtained are in agreement with those reported by Parida et al. [10]. The values decrease with increasing cation vacancy fraction x. This confirms the cation vacancy theory.

3.5. Electrochemical activity

The discharge tests of MnO_2 samples were carried at a constant current of 30 mA/0.5 g in an electrolyte containing $ZnCl_2$ and NH_4Cl (pH: 4.2) at room temperature. The results are summarized in Table 2 and presented in Fig. 4. As is generally known, the electrochemical activity of MnO_2 increases with increasing open-circuit potential (OCP) and initial discharge voltage plateaus as compared with the equi-

Table 1
Chemical analyses and formula of manganese dioxide samples

Sample	MnO_2 (%)	Mn (%)	x in MnO_x	Combined water (%)	Pycnometric density (g/cm^{-3})	n	m	x	y	Chemical formula			
										Mn_{1-x-y}^{4+}	Mn_y^{3+}	O_{2-4x-y}^{2-}	OH_{4x+y}^{-}
A_1	86.24	55.72	1.978	3.00	2.986	1.989	0.138	0.64	0.0205	$Mn_{0.915}^{4+}$	$Mn_{0.0205}^{3+}$	$O_{1.723}^{2-}$	$OH_{0.276}^{-}$
A_2	87.53	56.85	1.973	2.25	3.41	1.986	0.0969	0.046	0.0261	$Mn_{0.927}^{4+}$	$Mn_{0.0269}^{3+}$	$O_{1.788}^{2-}$	$OH_{0.211}^{-}$
A_3	85.82	56.97	1.952	1.78	3.80	1.976	0.064	0.031	0.0465	$Mn_{0.922}^{4+}$	$Mn_{0.0465}^{3+}$	$O_{1.829}^{2-}$	$OH_{0.170}^{-}$
B_1	83.42	54.80	1.948	2.55	3.28	1.974	0.100	0.047	0.0495	$Mn_{0.902}^{4+}$	$Mn_{0.0495}^{3+}$	$O_{1.76}^{2-}$	$OH_{0.239}^{-}$
B_2	69.98	51.43	1.86	5.43	2.67	1.93	0.2196	0.098	0.123	$Mn_{0.718}^{4+}$	$Mn_{0.123}^{3+}$	$O_{1.477}^{2-}$	$OH_{0.523}^{-}$
B_3	71.22	54.23	1.83	11.50	2.604	1.915	0.534	0.211	0.134	$Mn_{0.655}^{4+}$	$Mn_{0.134}^{3+}$	$O_{1.022}^{2-}$	$OH_{0.978}^{-}$
C	93.00	57.69	2.00	0.02	4.64	2.00	0.0008	0.00044		$Mn_{0.999}^{4+}$		$O_{1.998}^{2-}$	$OH_{0.0016}^{-}$

Table 2
Discharge characteristics of the manganese dioxide samples in $ZnCl_2 + NH_4Cl$ solution

Sample	Crystal phase	Open-circuit voltage (V)	Discharge time to 1.0 V cutoff (min)	Capacity (A s/g)
A_1	γ	1.552	232	1044
A_2	γ	1.546	220	990
A_3	γ	1.532	140	630
B_1	α	1.640	132	594
B_2	δ	1.568	104	468
B_3	δ	1.660	92	414
C	β	1.410	28	126

librium open-circuit voltages. It is now well established [22] that the sloping nature of the discharge curve, e.g. the continuous voltage decay is due to the take-up of protons and electrons, resulting in an accumulation of a lower oxide:

$$MnO_2 + H^+ + e^- \rightarrow MnOOH \quad (3)$$

The concentration of the formed MnOOH is also influenced by the disproportionation reaction:

$$2MnOOH + 2H^+ \rightleftharpoons MnO_2 + Mn^{2+} + 2H_2O \quad (4)$$

The total length of the discharge depends on the ability of the lattice to accommodate protons and to undergo the necessary expansion [22]. There are two main factors that affect the capacity of MnO_2: (i) the ability of the formation of lower oxides such as MnOOH (Mn^{3+}) according to Eq. (3), and (ii) the dependence on the acidity of the electrolyte supplying protons which initiates the transformation of lower oxides to MnO_2 (Mn^{4+}) according to Eq. (4). The electrochemical potential of the MnO_2 electrode depends on the Mn^{3+}/Mn^{4+} ratio. This ratio is determined by the form of MnO_2 used and therefore depends on the synthesis method [23]. The presence of Mn^{3+} in the same crystallographic positions as Mn^{4+} is stabilized by OH^- ions [24].

Samples A_1, A_2 and A_3 (γ-MnO_2) showed high OCP and long discharge plateaus (Fig. 4), indicating high activity which corresponds practically to the high quantity of electricity involved in the electrochemical reaction. On the other hand, samples B_1, B_2, B_3, which are characterized by poor activity, showed a lower OCP and a short plateau region (Fig. 4). This difference in the activity between the two sample groups A and B seems to be related to the difference in the combined water content and the Mn^{3+} concentration. As shown in Table 1 samples of group B containing high contents of lower oxides (Mn^{3+} ions) and high amounts of combined water have low activity. This means that the formation of Mn^{3+} in the same crystallographic position as Mn^{4+} is not possible for this group of samples.

These results coincide with those reported by Giovanoli [25], who stated that δ-MnO_2 behaves very different compared with the γ-variety, and that sheets of water molecules

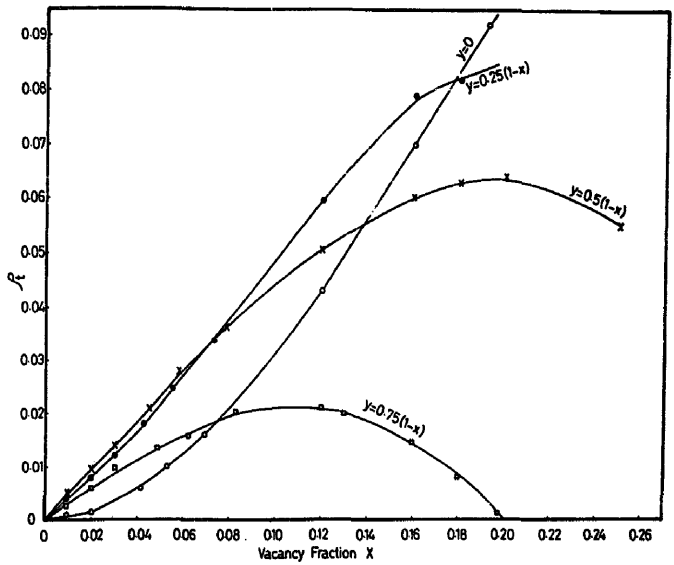

Fig. 4. Discharge curves of the manganese dioxides in $ZnCl_2 + NH_4Cl$ solution at 30 mA/0.5 g. (○) A_1, (△) A_2, (●) A_3, (×) B_1, (■) B_2, (▲) B_3, and (□) C.

or OH groups are located between the layers of edge-shared $[MnO_6]$ octahedral.

It may be recalled that for α-MnO_2 the O–H bending frequency is absent in the IR spectra, in spite of the fact that much water is present in this sample, as evidenced from its chemical formula, which calculated according to the cation vacancy model. This may be due to chemically bound water in the pores. This result is in agreement with that reported by Erdays et al. [26]. They stated that water is present in two forms, the first is loosely bound water and can be removed at 100 °C, and the second is strongly bound water, adhering to the pore walls. This result indicates that the cation vacancy model should not be applied to α-MnO_2 containing molecular water to calculate x from m.

For γ-MnO_2 samples (group A), which show high activity, y values (lower oxides) and water content are lower than the corresponding figures of group B samples. It appears that OH^- ions are present in conjunction with Mn^{3+} in the γ-MnO_2 structure. This permits diffusion of protons, associated with the change of Mn^{4+} to Mn^{3+}. Proton mobility is responsible for the increased activity of group A samples. Furthermore, it may be observed from Table 2 and Fig. 4 that the activity of group A samples increases with increasing vacancy fraction (x values). This may due to the fact that immobile protons associated with vacancies are assisting in the movement of protons by a proton-exchange mechanism. This conclusion is in agreement with that reported by Ruetschi and Giovanoli [21]. They stated that there are two types of protons, in the MnO_2 lattice: localized immobile (Ruetschi) protons, associated with vacancies, compensating the charge of the missing manganese ions (Mn^{4+}), and mobile (Coleman) protons, associated with Mn^{3+} ions, formed through introduction electrons during reduction. The proton transfer m (γ-MnO_2) is correlated mainly to the OH^- ions. The OH^- ions incorporated into the lattice, as a consequence of cation vacancies, will act as donors and provide thus an initial concentration of protons for solid-state proton transfer in terms of the reaction-rate theory; one may thus express the probability of proton transfer by:

$$P_t = \nu[OH^-][O^{2-}] \tag{5}$$

where ν is the jump frequency and $[OH^-]$ represents the concentration of proton-occupied sites, and $[O^{2-}]$ the concentration of available, suitable empty sites for proton transfer. The proton-transfer process, shall now be detailed for the case of ramsdellite structure. Two types of $[O^{2-}]$ and $[OH^-]$ sites must here be distinguished: the planar $[O^{2-}]_{pl}$, $[OH^-]_{pl}$ and the pyramidal $[O^{2-}]_p$, $[OH^-]_p$ configuration with respect to the three next-neighbour Mn^{4+} ions. Only the 'pyramidal' O^{2-} are suitable sites for proton uptake [27]. According to that reported by Reutschi [20], the rate of proton transfer (P_t) in the γ-MnO_2 could thus visualized as being proportional to:

$$P_t \approx [OH^-]_{pl}[OH^-]_p[O^{2-}]_p$$
$$= (4-P)_x(p_x+y)(1-P_x-y) \tag{6}$$

where $[OH^-]_{pl}$ and $[OH^-]_{pl}$ are the number of planar and pyramidal sites occupied by protons, present as a result of Mn vacancies, and $[O^{2-}]_{py}$ represents the total number of unoccupied pyramidal sites. This expression is plotted in Fig. 5 as a function of x, for $p=2$, and for several values of y as parameter [20]. According to Fig. 5, for small values of x and y, the rate of proton transfer increases with the cation vacancy fraction x and OH^- concentration y. x values greater than 0.25 could be detrimental. They would correspond to very high structural water contents [20,28], and would produce lower electrochemical activity. Thus, the rate of proton diffusion in the MnO_2 solid phase — if other parameters not

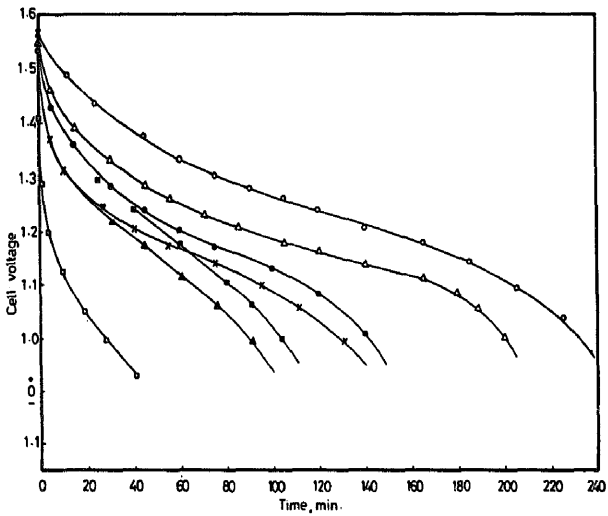

Fig. 5. Relative proton-transfer rate as a function of Mn^{4+} vacancy fraction x for γ-MnO_2.

related to structure such as porosity, particle size, electrolyte composition and nature, and the amount of conducting agent (graphite, carbon black) are kept constant — determines the activity. The above-mentioned results show that the presence of cation vacancies is an essential prerequisite for fast proton diffusion in γ-MnO_2.

For δ-MnO_2 high concentrations of vacancies and structural water are undesirable. Increasing the number of vacancies may lead to vacancy clustering, which affects greatly the lowering of the electrochemical activity [21].

4. Conclusions

1. XRD measurements with γ-MnO_2 samples showed that the number of lattice defects decreases with decreasing number of cation Mn vacancies, as derived from chemical analysis.
2. The γ-MnO_2 structure exhibiting high electrochemical activity contains cation vacancies. The charge of each missing Mn^{4+} ion in the lattice is compensated by four (localized) immobile protons. Immobile protons, associated with vacancies, will assist proton diffusion by a proton-exchange mechanism. Protons introduced during reduction become associated with O^{2-} to form OH^-.
3. The cation vacancy model should not be applied to material such as α-MnO_2 containing probably water in molecular form.

References

[1] E. Preisler, *J. Appl. Electrochem., 6* (1976) 301.
[2] S.B. Kanugo, K.M. Parida and B.R. Sant, *Electrochim. Acta, 26* (1981) 1147.
[3] B.B. Owens, B.K. Patel, P.M. Skarstad and D.L. Warburto, *Solid State Ionics, 9/10* (1983) 1241.
[4] J.B. Fernands, B.D. Desai and V.N. Kamat Dalal, *Electrochim. Acta, 29* (1984) 187.
[5] B.D. Desia, J.B. Fernandes and V.N. Kamat Dalal, *J. Power Sources, 16* (1985) 1.
[6] K. Kuwabara, H. Hanafusa and K. Sugigma, *J. Electrochem. Soc., 136* (1989) 319.
[7] N.D. Ivanova, S.A. Kirilov and A.B. Mishchenko, *Electrochim. Acta, 38* (1993) 2305.
[8] R.G. Burns and V.A. Burns, *Proc. Manganese Dioxide Symp., Cleveland, OH, USA, 1–2 Oct. 1975*, Vol. 1, The Electrochemical Society, Pennington, NY, USA, 1975, Paper No. 16.
[9] R.G. Burns, in A. Kozawa and M. Nagayama (eds.), *Battery Materials Symp., Brussels, Belgium, 1983*, BMRA, Cleveland, OH, USA, 1984.
[10] K.M. Parida, S.B. Kanungo and B.R. Sant, *Electrochim. Acta, 25* (1981) 435.
[11] A.I. Vogel, *Quantitative Inorganic Analysis*, 1981.
[12] J.P. Brenet, G. Coelfier and J.P. Gabano, *Electrochim. Acta, 8* (1963) 273.
[13] J.P. Brenet, M. Cyarankowska, G. Ritzier, R. Saka and K. Traore, *Symp. Manganese Dioxide, Cleveland, OH, USA, 1–2 Oct. 1975*, The Electrochemical Society, Pennington, NY, USA.
[14] A.J. Brown, F.L. Tye and L.L. Wood, *J. Electroanal. Chem., 122* (1981) 337–346.
[15] A.A. Abdul Azim, G.A. Kolta and M.H. Askar, *Electrochim. Acta, 17* (1972) 291.
[16] J.B. Fernandes, B. Desai and V.N. Kamat Dalal, *Electrochim. Acta, 28* (1983) 309.
[17] J.B. Fernandes, B. Desai and V.N. Kamat Dalal, *J. Appl. Electrochim., 15* (1985) 351.
[18] Y.-Y. Kharitonov and Yu.A. Buslaev, *Izv. Akad. Nauk. Ser. Ser. Chem.*, (1962) 393.
[19] E. Narita and T. Okabe, *Bull. Chem. Soc. Jpn., 53* (1980) 525.
[20] P. Ruetschi, *J. Electrochem. Soc., 131* (1984) 2737.
[21] P. Ruetschi and R. Giovanoli, *J. Electrochem. Soc., 135* (1988) 2663.
[22] N.C. Cahoon, in N.C. Cahoon and G.W. Heise (eds.), *Primary Batteries*, Vol. 2, Wiley, New York, 1976, p. 68.
[23] P. Ruetschi and R. Giovanoli, *J. Appl. Electrochem., 12* (1982) 109.
[24] J.P. Brenet, *J. Power Sources, 4* (1979) 183.
[25] R. Giovanoli, *Chimia, 23* (1969) 472.
[26] L. Erday, *Gravimetric Analysis*, Part 1, Macmillan, New York, 1983, p. 298.
[27] W.C. Maskell, J.E. Shaw and F.L. Tye, *Electrochim. Acta, 28* (1983) 225.
[28] J.B. Fernandes and B.D. Desai, *J. Power Sources, 34* (1991) 207.